Rev.Adv.Mater.Sci. 5 (2003) 270-280

EFFECTS OF ENERGETIC SPECIES DURING THE GROWTH OF BORON NITRIDE AND AMORPHOUS CARBON THIN FILMS BY SPUTTER DEPOSITION

S. Logothetidis

Aristotle University of Thessaloniki, Department of Physics, Solid State Physics Section, GR-54124 Thessaloniki, Greece

Received: July 25, 2003

Abstract. We study the effect of Ar^+ irradiation during the growth of BN and a-C by sputter deposition. We found that the dominant effects for the BN growth are the subplantation of N^+ and B^+ species. For energies higher than the threshold for Ar^+ subplantation, Ar^+ penetrates into BN and disrupts the B-N bonds resulting to defective BN. The existence of Ar impurities in such films promotes the stability of C impurities. These effects result to a very narrow window of ion energy (<40 eV) were successful growth of BN films may be achieved. On the other hand, in a-C films sp^3-bonded C we found a close correlation between the Ar impurities with the sp^3 C-C bonds, which suggest that Ar impurities promote the formation of sp^3-bonded carbon in a-C, in contrast to BN growth. In addition, it was found that the films grown using C^+ (Ar^+) exhibit a sp^2 (sp^3) surface, while the deeper monolayers are sp^3 (mixed sp^3-sp^2) bonded. We found two mechanisms of sp^3 formation: on the surface and in the bulk of a-C. We conclude that at medium energy (>100 eV) the surface effects are negligible (for both C^+ and Ar^+), while the surface processes dominate when low-energy (~40 eV) Ar^+ ions are used.

1. INTRODUCTION

Boron Nitride (BN) and amorphous Carbon (a-C) are two materials, which meet the requirements for use in protective coatings for high technology applications such as optical systems and magnetic recording media [1,2]. They share many similar properties such as the type of bonding (sp^2 or sp^3), the tetrahedral character of sp^3 bonds, ultra-high hardness and optical transparency. The growth of sp^3-bonded BN or a-C can be achieved only under intense ion irradiation conditions. Magnetron sputtering (MS) is a simple, versatile growth technique, which uses energetic ions and can be applied in large-scale deposition. Although the growth of highly tetrahedral a-C (ta-C) by MS is still questioned, MS can grow a-C films with considerable sp^3 content and ultra-smooth surfaces and interfaces [3,4]. In the case of BN, MS at high temperatures (>300 °C) has been successfully applied to the growth of cubic BN (sp^3-bonded) [5]. We have recently shown that MS at room temperature (RT) can grow partly sp^3-bonded BN films and to prevent crystallization, resulting to homogeneous a-BN with high-hardness and ultra-smooth surfaces and interfaces, similar to sputtered a-C [6,7].

The studies of BN and a-C growth have been focused to bulk processes like the subplantation and densification (SD) mechanisms, which are due the depositing energetic species (B^+, N^+,C^+). However, in the case of sputter deposition of sp^3-bonded a-C and BN films the incorporation of non-depositing energetic species, such as inert gas ions (mainly Ar^+), enhance the surface effects during growth, which have not gained much attention so far. In addition the non-depositing species may modify the local structure in the films and change the diffusion and thermalization processes [1,2].

Corresponding author: S. Logothetidis, e-mail: logot@auth.gr

In this work we study the effect of Ar^+ irradiation during the growth of BN and a-C by sputter deposition. X-ray Photoelectron Spectroscopy (XPS), Auger Electron Spectroscopy (AES), X-Ray Reflectivity (XRR), Spectroscopic Ellipsometry (SE) and Fourier Transform IR SE (FTIRSE) are used to study their structural properties. Additional stress measurements were performed to identify the effect of the film stress and to correlate them with the other properties of BN and a-C. XPS has been also used to determine the content of Ar impurities.

We have found that the sputter deposition of BN and a-C does not follow exactly the same overall trends. Thus, for BN it was found that the dominant effects for the c-BN growth are the subplantation of N^+ and B^+ species, which follow very well the SD model for ion energies below the threshold of Ar^+ subplantation into BN. The film stress follows the prediction of the SD model for films with stress higher than a stress threshold of 3.5 GPa. For energies higher than the threshold for Ar^+ subplantation, Ar^+ penetrates into BN and disrupts the B-N bonds resulting to defective BN.

The existence of Ar impurities in such films retains the high stress (larger than it would be expected for films with low sp^3 content) and promotes the stability of C impurities and the formation of C-N bonds. These effects result to a very narrow window of ion energy (<40 eV) were successful growth of c-BN films may be achieved. On the other hand, in a-C films sp^3-bonded C we found a close correlation between the Ar impurities with the sp^3-content which suggest that Ar promotes the formation of sp^3-bonded carbon in a-C. Finally, it was found that the films grown using C^+ (Ar^+) exhibit a sp^2 (sp^3) surface, while the deeper monolayers are sp^3 (mixed sp^3-sp^2) bonded. These results were compared with simulations of the ion-solid interactions and the results of a phenomenological model which takes into account the balance between the surface and bulk processes. We found two mechanisms of sp^3 formation: on the surface and in the bulk of a-C. We conclude that at medium energy (>100 eV) the surface effects are negligible (for both C^+ and Ar^+), while the surface processes dominate when low-energy (~40 eV) Ar^+ ions are used.

2. EXPERIMENTAL DETAILS

The a-C (BN) films were deposited by *RF* MS using 6 in. hot pressed graphite (h-BN) target – 99.999% purity – in a high vacuum chamber (P_b <1·10^{-7}mbar). The details of the a-C and BN growth were described in Refs. [3,4,6,7]. Deposition at RT is essential to prevent BN crystallization. The energy and the flux of the ions varied by applying an external bias voltage (V_b) to the substrate in the range +10 V (self bias) to –170 V. The *RF* plasma characteristics were evaluated through current-voltage (*I-V*) measurements acquired by a Langmuir probe in the range –60 to +60 V using a tungsten tip.

Ex-situ SE measurements were obtained in the energy region 1.5-6.5 eV with a step of 20 meV. The FTIRSE measurements were performed ex-situ in the spectral range 900-4000 cm^{-1}, with a step of 8 cm^{-1}, using a phase modulated IR ellipsometer at 70^o angle of incidence.

Stress measurements were performed by measuring their curvature [8]. XRR measurements were described in Refs. [4,6]. XPS spectra were acquired using monochromated Al-K_α (1486.5eV) X-radiation, and a hemispherical analyser at pass energy of 50 eV. The energy resolution at 50 eV is 0.88 eV as it was estimated from the full width at half maximum of the XPS Ag $3d_{5/2}$ of a pure Ag target. The X-ray excited AES (XAES) measurements were acquired in another UHV chamber (P_b=3·10^{-10} Torr). A hemispherical electron energy analyzer, a twin anode X-ray source (unmonochromatized MgK_α line at 1253.6 eV) and a constant pass energy of 97 eV for the analyzer were used, giving a half width at half maximum of 1.6 eV for the Ag $3d_{5/2}$ peak.

3. RESULTS AND DISCUSSION

3.1. Structure and growth mechanisms of BN films

The BN films grown at RT using mixed Ar/N_2 sputter gases are amorphous [6,7]. Their amorphous character has been identified by X-Ray and Electron Diffraction patterns [6,7]. Fig. 1 shows a representative XRD diffractogram from an amorphous BN film, where the characteristic intense XRD peaks of c-BN and h-BN are strikingly missing. However, these films are denser than h-BN (as we will discuss below) suggesting that are partly sp^3 bonded. The growth of amorphous, sp^3 bonded BN films provides many advantages for applications where film homogeneity is essential [6,7].

For a more detailed study of the BN film microstructure, we also examined by FTIRSE the BN films named #A (sp^2-bonded) and #B (mixed sp^2/sp^3). FTIR spectroscopy is a technique that has been proved to be a powerful tool in identifying the bonding and the phases of BN [9]. The FTIRSE technique is capable of direct determination of the material's complex dielectric function and the iden-

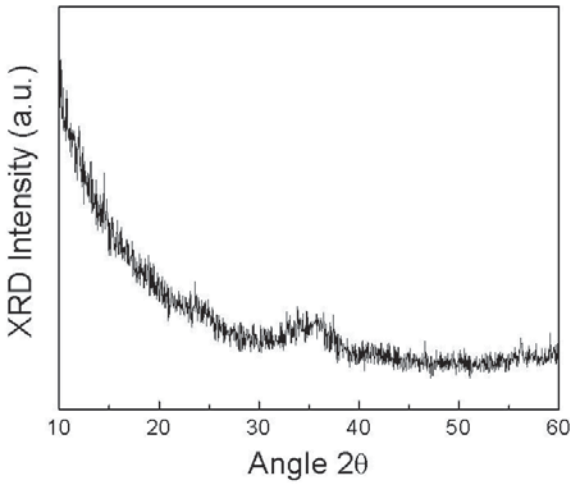

Fig. 1. X-Ray diffractogram from a representative BN film, revealing its amorphous character.

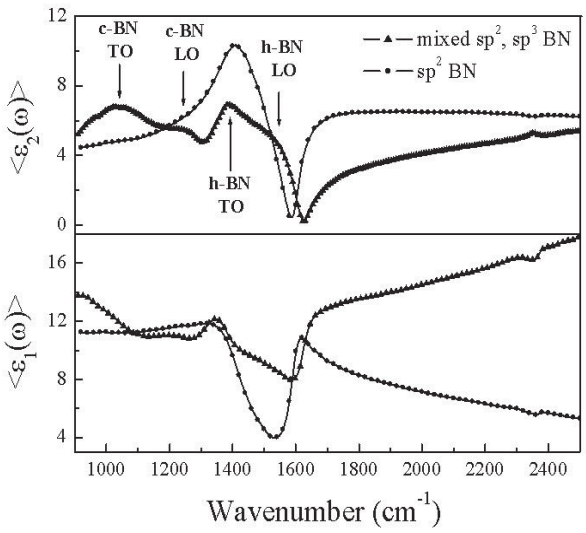

Fig. 2. Representative FTIRSE spectra of sp^2-bonded and mixed sp^2/sp^3 BN films. Arrows denote the characteristic bands of the IR-active B-N chemical bonds that correspond to h-BN and c-BN phases (crystalline counterparts of sp^2 and sp^3 BN, respectively).

tification of chemical bonds even with low IR response due to its high sensitivity [9]. Every IR-active bond contributes to the FTIRSE spectra with a characteristic vibration band, which can be modelled by a Lorentz oscillator. Fig. 2 presents the FTIRSE spectra of the aforementioned composite BN films. The $\varepsilon(\omega)$ spectrum of film #A is dominated by two characteristic bands corresponding to the TO- and LO-mode of h-BN at 1367 and 1610 cm^{-1}, respectively, revealing, its sp^2 character, taking into account that h-BN is the crystalline counterpart of sp^2-bonded a-BN. On the other hand in the e(w) spectrum of BN film #B, in addition to h-BN bands, the characteristic bands corresponding to the TO- and LO-mode of c-BN at 1056 and 1305 cm^{-1} appear, revealing the pronounced sp^3 character of the film (again c-BN is the crystalline counterpart of sp^3-bonded a-BN). The FTIRSE results are also supported by XRR data analysis, which determines the BN films density, trough which the sp^3 content can be estimated [9].

Information on the density, thickness, and surface roughness of BN films is deduced by XRR through the dependence of the reflection coefficient on the angle of incidence. The XRR measurements were analyzed using a Monte–Carlo (MC) algorithm assuming a single layer of stoichiometric BN (Fig. 3). There is very good agreement between experimental and fitting results with the one layer model proving the homogeneity of the BN films [6]. The surface roughness has been determined by XRR. In all cases the roughness of the presented BN_x films is in the range of 0.3–0.5 nm. The calculated film density depends slightly on the ratio *Z/A* of the mean atomic number *Z* to atomic mass A and a correction in the XRR results is required [6]. However, this correction is well below 2% for the wide range $0.4<x<2$, so that it does not affect the validity of the MC fit results [6]. The BN film density can be used as a criterion of the sp^3 content in a-BN, since in most cases it is higher than the density of the h-BN (2.3 g cm^{-3}). The BN film density versus V_b is presented in Fig. 4a. The BN films deposited at V_b=0 V exhibit density below 2.3 g cm^{-3} indicating that they are mostly sp^2-bonded and consistent with the random distribution of sp^2 sites. On the other hand, all the films deposited with negative V_b are considerably denser than h-BN suggesting the formation of sp^3 a-BN in the films and the elimination of voids, in agreement with FTIRSE results.

According to the film density (Fig. 4a), the optimum V_b for the formation of sp^3 bonded a-BN by sputter deposition is approximately -60 V, in agreement with previous studies suggesting a similar ion energy to be the most suitable for the nucleation of sp^3-bonded c-BN [10]. Comparing the required ion energy for the nucleation of c-BN [10] with the one required for the formation of sp^3 a-BN we conclude that the ion energy alone is responsible for the transformation of the sp^2 phase to sp^3 BN, while the sub-

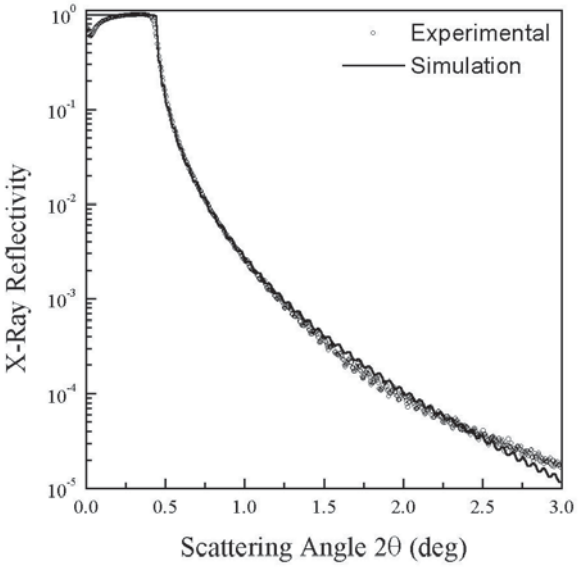

Fig. 3. A representative XRR curve from a sputtered BN film, with a density of 2.4 g/cm^3 and the simulated XRR curved based on the results of the MC fit.

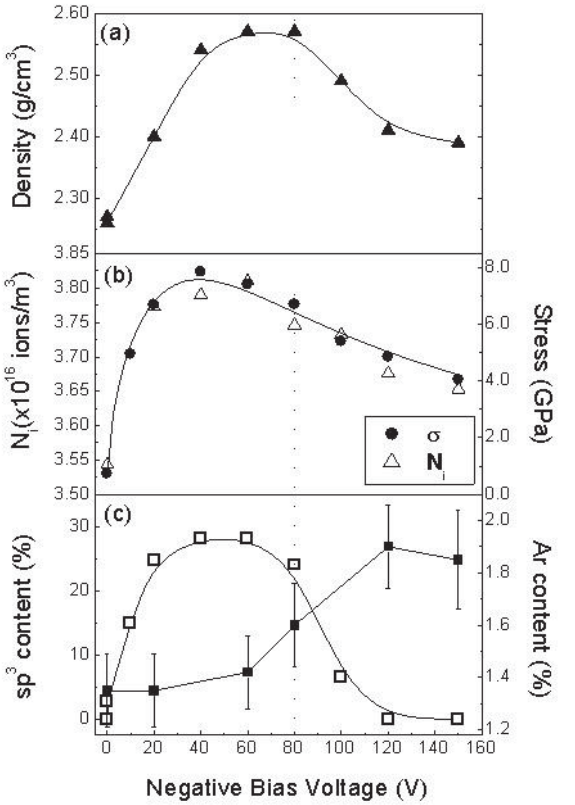

Fig. 4. The variation of (a) mass density (determined by XRR), (b) density of ions N_i, and internal stress σ, and (c) sp^3 and Ar content, of BN films vs V_b (ion energy).

strate temperature is responsible for the local rearrangement of sp^3-BN atoms and the transformation of the amorphous sp^3-BN to crystalline c-BN.

XPS provided the chemical analysis of the a-C and BN surfaces. The characterization was derived from the spectra of wide scan and from the spectra of peaks B1s, N1s, C1s, and O1s. The C1s peak manifested due to the C impurities on the BN surface. After sputter cleaning of the BN surface, the C1s peak disappeared, except in the case of films grown at $|V_b|$>100 V. In the later case, the C impurities are incorporated in the bulk of BN, as well. It is known that the BN films containing sp^2 and sp^3 bonds have discernable features in XPS. Both sp^2– and sp^3-bonded BN films exhibit bulk plasmon loss peaks at approximately 25 and 27 eV, respectively, below the B1s and N1s peaks. However, due to the difference in bonding energies between sp^2 and sp^3 BN, the sp^2 -bonded BN exhibits the additional p plasmon loss peak at approximately 9eV below the B1s and N1s peaks. The presence of this feature is a 'fingerprint' of sp^2-BN [11].

XPS provided the chemical analysis of the a-C and BN surfaces. The characterization was derived from the spectra of wide scan and from the spectra of peaks B1s, N1s, C1s and O1s. The C1s peak manifested due to the C impurities on the BN surface. After sputter cleaning of the BN surface, the C1s peak disappeared, except in the case of films grown at $|V_b|$>100 V. In the later case, the C impurities are incorporated in the bulk of BN, as well. It is known that the BN films containing sp^2 and sp^3 bonds have discernable features in XPS. Both sp^2– and sp^3-bonded BN films exhibit bulk plasmon loss peaks at approximately 25 and 27 eV, respectively, below the B1s and N1s peaks. However, this analysis is very difficult due to the low broadening B1s and N1s peaks. Nevertheless, the sp^3/sp^2 ratios in BN films determined by XPS [7] exhibit the same qualitative variations vs V_b (ion energy) with the ratios determined by FTIRSE, SE and through the density values of BN (determined by XRR). However, this comparison shows that XPS overestimates the sp^3 content in the case of BN films. Finally, the content of Ar impurities in the a-C and BN films has been determined from the XPS wide-scan spectra comparing the area of the Ar2s and Ar2p with the C1s (for a-C) B1s and N1s peaks (for BN).

SE in the vis-UV spectral region, was also used for phase and bond-structure identification of a-C

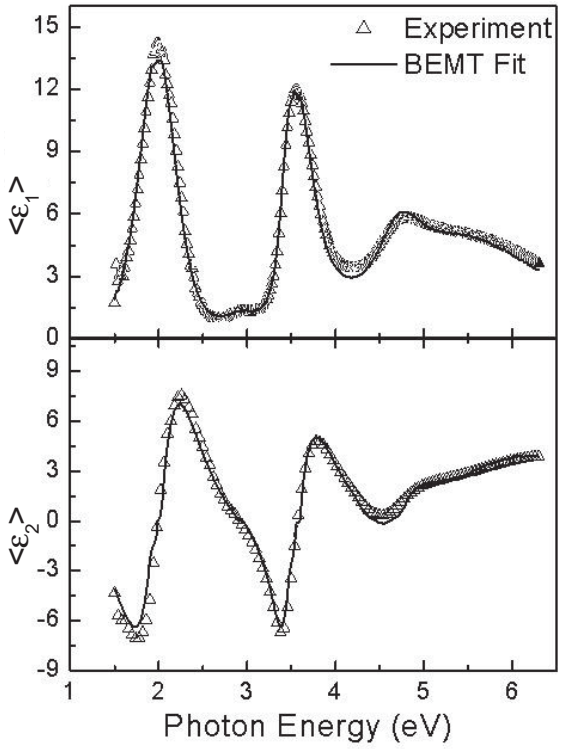

Fig. 5. Representative SE spectra from a BN film, 170 nm thick, and the corresponding BEMT fit.

and BN [3,4,6,7]. SE is a widely applied and non-destructive surface-sensitive technique, which determines the complex dielectric function $\varepsilon(\omega) = \varepsilon_1(\omega) + i\varepsilon_2(\omega)$. The $\varepsilon(\omega)$ is directly related to the electronic properties, the chemical bonding as well as the structural and the morphological properties of the materials. In the case of a thin film grown on a bulk substrate, the measured quantity by SE is the pseudodielectic function $\langle\varepsilon(\omega)\rangle$ that accounts the effect of the substrate and film's thickness in addition to the film's dielectric response. In order to deduce the bulk $\varepsilon(\omega)$ by a fitting procedure, the appropriate model should be applied.

Therefore, SE can also determine the volume fractions of sp^3- and sp^2-bonded BN through analysis with the Bruggeman Effective Medium Theory (BEMT) [12,13]. Fig. 5 shows the $\langle\varepsilon(\omega)\rangle$ spectra (open triangles) of a representative BN film, 170 nm thick, and the corresponding BEMT fit results (solid lines). We observe that the BEMT fit is very accurate both in the region of optical transparency (multiple reflections below 4.5 eV) and in the region of optical absorption (>4.5 eV), showing that it describes very well the refractive index and the interband transitions of BN, as well. However, the sp^3 content of BN determined by BEMT results does not exhibit a strong, linear correlation with the film density (see Fig. 4c), as it has been observed in the case of a-C [14]. This is attributed to the existence of small grains of h-BN and c-BN in the BN films, as well as to the impurities in BN for high ion energy (negative V_b). Nevertheless, both the sp^3 content determined by BEMT and the BN density exhibit a behavior typical of the SD process during growth [1], with a narrow window of 30-40 eV, where sp^3 bonds are formed.

Another important property for the study of the growth of BN films is the internal stress. The internal stress was determined by the bending method and calculated from Stoney's equation [8]. Fig. 4b shows that the a-BN films exhibit stress greater than the Berman–Simon phase boundary (3.5 GPa) [15], similar to c-BN films. According to the presented stress variation vs V_b, there is a window of V_b where the sp^3 bonds dominate and this leads to high compressive stresses. The same variation with V_b follows the density of ions N_i (Fig. 4b, open triangles), revealing the close correlation between the internal stress and the density of ions.

The stress behaviour of BN films is typical for a SD process during growth. The stress variation of films grown with a SD process is described by the formula of Davis [1,16,17]:

$$\sigma = \frac{Y}{1-\nu} \cdot \frac{\sqrt{E}}{\frac{\Phi_n}{\Phi_i} + k \cdot E^{5/3}}, \qquad (1)$$

where Φ_n/Φ_i is the relative flux of neutral to ionized species, Y is film's Young modulus, ν is the Poisson ratio, E is the ion energy and k is a parameter, which accounts the effect of outdiffusion of the implanted, hyperthermal species from the bulk to the film surface (a process usually called thermalization). Application of Davis model (solid line in Fig. 4b) in our experimental results shows that the model describes very well BN and confirms that the growth of BN is based on a SD process.

A special feature of sputter deposition is the incorporation of inert gas (Ar) impurities [4]. The ion density in the plasma during growth is presented in Fig. 4b (open triangles). We note here that this density of ions includes the contributions of Ar^+, B^+, N^+ and thus can not be exclusively correlated with the Ar^+ ions. The content of Ar impurities determined by XPS from the area of the Ar2p, B1s, and N1s peaks. Fig. 4c shows the variation of Ar content in

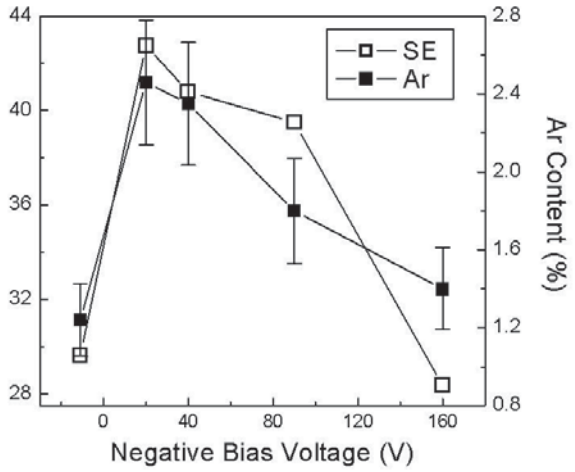

Fig. 6. The variation of the sp^3 and Ar content, of a-C films vs V_b (ion energy).

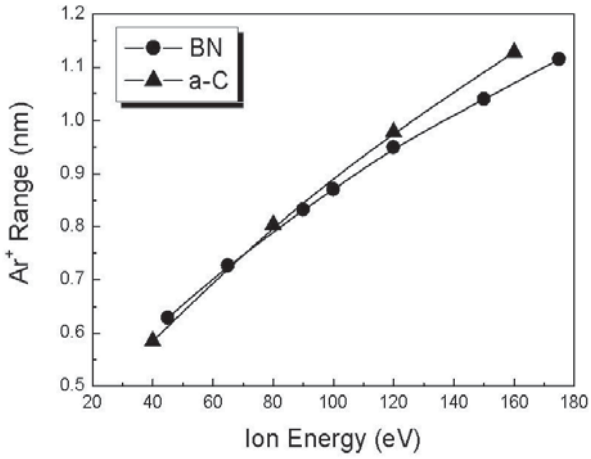

Fig. 7. The Ar^+ penetration depth into BN and a-C vs ion energy calculated by SRIM.

the BN films vs V_b determined by XPS and sp^3 content measured by SE. The SE results regarding the sp^3 content were chosen as more representative of the bulk properties of the films. We observe no correlation between the sp^3 content and the Ar impurities for BN films. In Fig. 4c the vertical dotted line indicates the V_b, which corresponds to the ion energy threshold for the Ar^+ subplantation, as it was determined by SRIM [18]. We observe that for V_b above the calculated Ar^+ subplantation threshold the Ar content in the BN films is considerably increased, supporting the SRIM computational results, while the content of sp^3 bonds is reduced even below the prediction of the SD model (see also Fig. 4c). Taking into account that the BN growth is based on the SD mechanism, we conclude that the constructive subplanted species are B^+ and N^+, while Ar^+ are destructive species, which disrupt the B-N bonds, but retain the high stress (Fig. 4b). In addition, Ar promotes the stability of C impurities, as it is detected by the C1s peak in XPS wide-scan spectra, which manifests even after sputter etching of the BN films' surface.

3.2. Structure and growth mechanisms of a-C films

The correlation between the Ar impurities and the sp^3 bonded material is the basic difference between the BN and a-C growth by MS. While in the BN case the subplantation of Ar^+ is destructive and disrupts the B-N bonds, for a-C the Ar^+ subplantation is beneficial and closely related with the sp^3 content in the films, as it is shown in Fig. 6. The Ar content in Fig. 6 has been determined by comparing the area below the Ar2p and C1s XPS peaks in the XPS wide-scan spectra and the sp^3 content has been determined by SE, which provides information about the bulk properties of a-C and is less affected by the surface phenomena [3,4]. The Ar concentration [Ar] varies between 1.2 and 2.6%. It is very interesting that there is not a monotonous increase of [Ar] with V_b but there is a maximum at low V_b coinciding with the maximum in sp^3 content as it was calculated by SE/BEMT [3,4] (the SE results regarding the sp^3 content were chosen again as more representative of the bulk properties of the a-C films), supporting the beneficial effect of Ar^+ subplantation to the transformation of sp^2 sites to sp^3, possibly due to the very high local strain and stress induced by the large Ar atoms into the a-C network.

Two possible explanations of the decrease of [Ar] for high V_b are considered; the first is due to the XPS analysis depth. In XPS measurements the information originates from the film surface, therefore, the observed [Ar] decrease at high V_b may by due to the corresponding high energy of Ar^+, which results to long penetration depth of subplanted Ar^+, beyond the analysis depth of XPS. In order to investigate this possibility for both BN and a-C we determined the mean penetration depth (ion range) of Ar^+ into a-C and BN using SRIM [18]. The results of SRIM calculations (Fig. 7) show that the penetration depth of Ar^+ into a-C and BN is below 1.2 nm in the energy range used. The calculated penetration depth is far below the analysis depth of the Ar2p

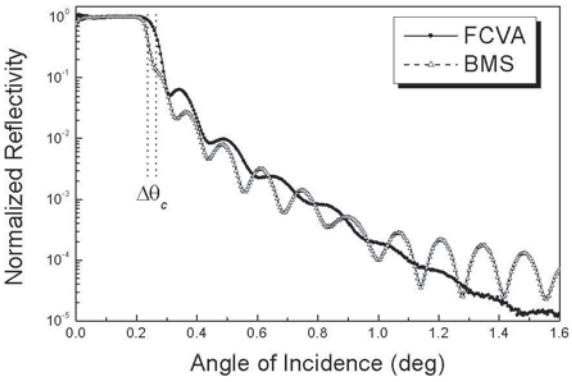

Fig. 8. Representative XRR curves for two a-C films, grown by FCVA and biased MS (BMS).

Table 1. Summary and comparison of the properties of BMS- and FCVA-grown a-C films determined by XRR.

Deposition Technique	BMS	FCVA
Density (g/cm^3)	2.62	3.23
Surface roughness (nm)	0.2	0.6
a-C/Si interface roughness (nm)	0.3	1.1
Thickness (nm)	32.7	24.9

and C1s XPS peaks, which is determined to be about 3 nm [3]. Therefore, the observed reduction of [Ar] at high V_b for a-C is due to Ar removal. Secondly, the Ar removal is possibly due to the preferential outdiffusion to the film surface of the weakly-bonded Ar atoms during the thermalization process of the SD mechanism [1].

We have shown that the depositing (B,N) and non-depositing (Ar) energetic species during deposition result to different effects and growth mechanism of a-BN films. In order to investigate the different effects due to depositing (C^+) and non-depositing (Ar^+) energetic species we compare the structure, morphology and growth mechanisms of a-C films grown by different physical vapor deposition (PVD) techniques such as MS, electron beam evaporation (EBE) and filtered cathodic vacuum arc (FCVA) [3].

The sp^3/sp^2 of all the a-C films content can be calculated by the film density r [4,14] using the density of an sp^2 bonded evaporated a-C thick film (ρ_{sp2}) and the density of crystalline diamond (ρ_{sp3}). This is because the sp^3 content and mass density of a-C films has been found to exhibit a linear correlation [4,14]. Therefore, the sp^3 content in a-C films can be calculated from XRR data analysis through the formula:

$$sp^3(\%) = 100 \times \frac{\rho_{sp^3} - \rho}{\rho - \rho_{sp^2}}. \qquad (2)$$

Fig. 8 shows representative XRR curves acquired from two a-C films (BMS- and FCVA-grown). The variations of the critical angle ($\Delta\theta_c$) are attributed to the variations of density. The FCVA-grown sample is the densest of all films and follows well the density values predicted for the SD mechanism of growth [2,19]. The BMS-grown sample is an intermediate case between the graphitic EBE film and the tetrahedral FCVA film. This shows that in the BMS growth there is a mechanism of sp^3 formation but it is not exactly the same with the one of the FCVA growth. The BMS-grown sample exhibits stronger interference fringes showing the better quality of the film surface and of the a-C/Si interface. This is attributed to the lower mobility and energy of the used Ar^+ ions in comparison with the C^+ ions used in the FCVA growth. Thus the C^+ ions penetrate more in the Si and a-C producing higher ion damage than Ar^+. On the other hand, Ar^+ affects only the top 1-2 monolayers (ML), as we will discuss in more details below, producing very sharp surfaces and interfaces. The sharp surface is an indication of a surface mechanism during growth in addition to the bulk SD. The quantitative results concerning these two films are summarized in Table 1.

The a-C films were also measured by AES and XPS in order to get direct information on their chemical state. The sp^3 content in the films was determined by AES using the C_{KLL} broadening ΔE taking into account the corresponding values ΔE_{sp2} and ΔE_{sp3} for graphite and diamond being 14 and 22 eV [20,21], respectively. AES confirmed the graphitic nature of the EBE-grown film and identified a highly-tetrahedral surface on the BMS-grown film. However, the densest FCVA sample exhibits a very broad C_{KLL} peak (not shown), which corresponds to sp^2 C. This is due to the different sampling depth of AES and XRR and it is attributed to the hybridization profile of the film, as we will discuss below. XPS has shown that the a-C surface incorporates mainly O

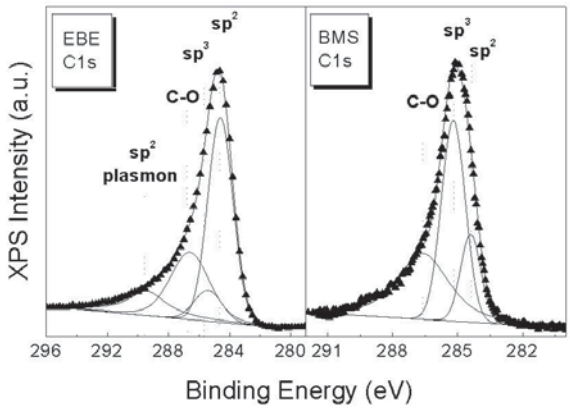

Fig. 9. Representative XPS spectra of the C1s peak for representative EBE- and BMS- grown films. In addition to the experimental curve, the deconvolution to the sp^3, sp^2, C-O, and sp^2-plasmon peaks and the baseline are shown.

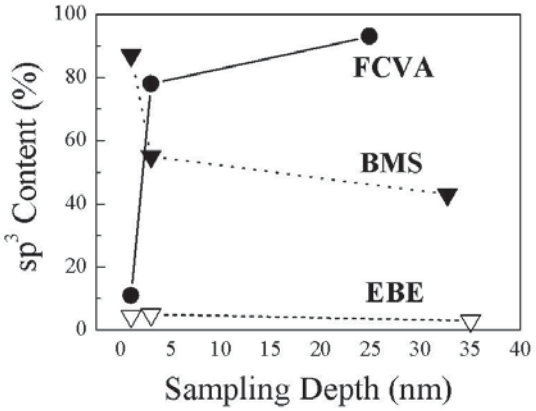

Fig. 10. The hybridization profiles of various a-C films determined by probing at different sampling depth. The points at 1, 3 nm correspond to AES and XPS data, respectively, and the bulk property (total film thickness) comes from XRR.

impurities (~10 %) and very low concentration of Ar, N, and Si as identified by the O1s, Ar2p, N1s and Si2p XPS peaks. The Ar concentration in the films, calculated by the Ar2p XPS peak, was strongly correlated with the sp^3 content in the BMS-grown films [4] supporting the considerations for ion-induced transformation of sp^2 sites to sp^3. Fig. 9 shows typical high-resolution XPS spectra of the C1s peak from a-C films deposited by BMS with V_b= -40 V and by EBE. The XPS spectra of the a-C films have been fitted with three components, which correspond to sp^2 bonded carbon, sp^3 bonded carbon, and C impurities (C-O bonds) [4,21]. In the case of highly graphitic films a fourth peak appeared due to plasmon energy losses of sp^2 C [21].

XRR, XPS and AES have different sampling depth. XRR's probe is the X-ray photons, which penetrate in the whole film. The sampling depth of XPS and AES depends on the escape depth of the excited electrons from the material. Thus, the electrons from the C1s (C_{KLL}) XPS (AES) peak have kinetic energy ~970 (~280) eV, which correspond to escape depth of ~3 (~1) nm [22]. Fig. 10 presents the hybridization profiles of the various a-C films as determined by AES/XPS/XRR. The EBE film is homogeneously graphitic. The FCVA film exhibits a highly-graphitic surface, while the sp^3 bonds are dominant in the bulk. This is in perfect agreement with the predictions of the SD model [2,19] and confirms the ta-C hybridization profiles reported by Davis *et al*. [23]. The most interesting case is the BMS-grown films that show a highly tetrahedral surface, which is not expected according to the so far proposed mechanisms of sp^3 formation.

In order to identify the differences between the FCVA- and BMS-grown a-C films, in Fig. 11 we compare the sp^3 content in the bulk vs the ion energy following the reports of Chhowalla *et al.* [24] and Logothetidis *et al*. [25], respectively. The data of Fig. 11 are comparable with the results of the films studied in this work, since the films in Refs. 24,25 have been grown with similar conditions with the presented films. In Fig. 11 we observe that for medium ion energy (>100 eV) both the FCVA- and BMS-

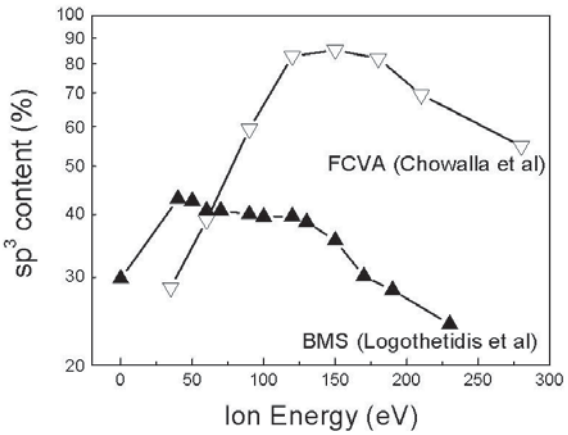

Fig. 11. The variation of sp^3 content for the FCVA and BMS growth of a-C.

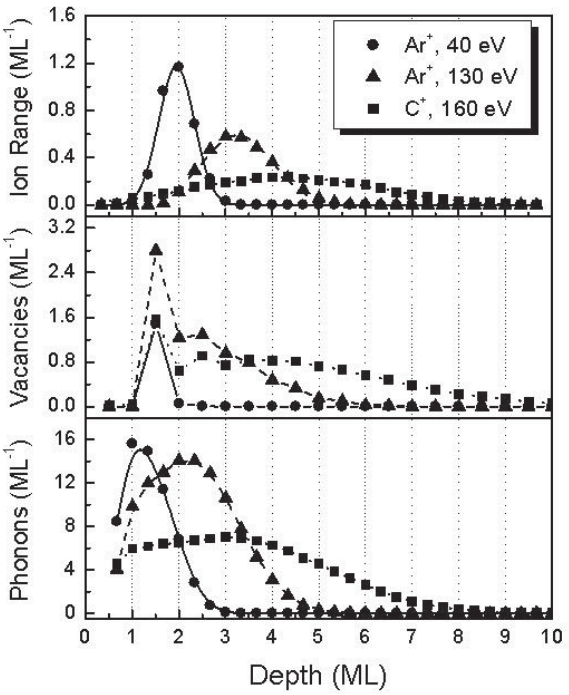

Fig. 12. SRIM calculations of the ion ranges of Ar^+ and C^+ ions into a-C and the distributions of the produced vacancies and phonons.

grown films exhibit the same qualitative behaviour with a maximum at 130-160 eV, which follows the prediction of the SD model. The difference in the absolute values between the two techniques is attributed to the relative flux of ions to the growing surface [2,3]. In the case of BMS and for low ion energy (<50 eV) a second peak appears, suggesting that an additional mechanism exists, which supports the SD and results to higher sp^3 content than it would be expected by the SD-mechanism alone.

The results shown in Fig. 11 regarding to the tetrahedral surface of the BMS sample suggest that the surface activated atoms may contribute to the surface formation of sp^3 bonds in this case. In order to identify the differences in the ion-solid interactions between the BMS and FCVA growth we performed a series of SRIM [18] calculations of the ion, phonon and vacancy distributions in the films during growth (shown in Fig. 12). For the calculations we used Ar^+ ions of 40 and 130 eV to simulate the two maxima of the BMS curve of Fig. 4, and C^+ ions of 160 eV to simulate the maximum of the corresponding FCVA curve. In the case of C^+ and medium-energy Ar^+ ions the bulk effects dominate as the maxima of all distributions are at depths of 4-5 monolayers (ML). The only difference between C^+ and Ar^+ ions in this high-energy regime is the wider distribution of ion damage in the case of C^+. Thus, the energy dissipation takes place in a narrower region in the case of Ar^+ making the thermalization effects [2,3,4] stronger, contributing to the degradation of the total sp^3 content. Considering the second maximum in the BMS curve of Fig. 11 and the similar ion damage produced by Ar^+ and C^+ ions we conclude that the SD-mechanism valids for BMS as it does for the FCVA growth. The qualitative difference, when low-energy Ar^+ ions are used, is the surface activation of C atoms. In this case the ion damage is concentrated on the surface (depth <2 ML). Especially, the produced vacancies are located exclusively on the surface, in perfect agreement with calculations of the surface and bulk vacancies following the formulation of Ref. 26, which show that the bulk vacancies start to appear for Ar^+ energy >60 eV. Therefore, in this energy regime the surface activation effects dominate, explaining the highly-tetrahedral surfaces of the BMS sample (Fig. 10).

Based on the previous experimental and computational results we developed a phenomenological model, which has been described in detail previously [27]. We used the variations of deposition rate to identify the various stages of film growth and to determine physical parameters such as the activation probability of C surface atoms, the rate of sp^3 formation on the surface, the ion implantation probability B and the probability λ of movement of bulk C atoms to the surface according to the thermalization mechanism [2,27]. The two latter parameters (B,λ) define the strength of SD-mechanism in forming sp^3 bonds in the bulk [27]. In the case of high B and λ the bulk effects dominate resulting to an sp^3 distribution [27] similar to that of the experimental FCVA-samples. As B and λ decrease the balance between surface and bulk effects changes in expense of the SD-mechanism resulting to lower sp^3 values and two distinct maxima [27] similar to the experimental curve of BMS-grown films in Fig. 11.

3. CONCLUSIONS

In this work we study by XPS, XRR and SE the effect of Ar^+ irradiation during the sputter growth of BN and a-C and the incorporation of inert, non-depositing Ar atoms into a-C and BN. Additional stress measurements were performed to identify the effect of the film stress and to correlate them with the other properties of BN and a-C. We have found that the conditions of Ar^+ irradiation during sputter depo-

sition of BN and a-C do not result to the same effects. Thus, for BN it was found that the dominant effects are the subplantation of N^+ and B^+ species, which follow very well the SD model for ion energies below the threshold of Ar^+ subplantation into BN. For energies higher than the threshold for Ar^+ subplantation, the Ar^+ penetrate into BN and disrupts the B-N bonds resulting to defective BN. On the other hand, in a-C films, the sp^3-bonded C we found a close correlation between the Ar impurities with the sp^3-content which, suggest that Ar impurities promote the formation of sp^3-bonded carbon in a-C, in contrast to BN growth. The removal of Ar in a-C films at high ion energy is attributed to the preferential outdiffusion of the weakly bonded Ar atoms during thermalization. Finally, we studied the differences in microstructure, morphology and growth mechanism of a-C films grown by different PVD techniques, which use C^+ and Ar^+ ions and we identified the differences introduced by the Ar^+ ions. The different sampling depth of AES/XPS/XRR enabled the accurate determination of their hybridization profiles, which are different due to the different ion-solid interactions and growth mechanisms. The experimental results have been compared with SRIM simulations showing two competing mechanisms of formation of sp^3 bonds on the surface and in the bulk of a-C. Based on these results we conclude that at the medium energy regime (>100 eV) the surface effects are negligible (whether the ions are C^+ or Ar^+), while the surface processes dominate when low-energy (~40 eV) Ar^+ ions are used, resulting to films with very smooth surfaces and interfaces.

4. ACKNOWLEDGEMENTS

The author gratefully acknowledges: Dr P.A. Patsalas (AUTh) for his long collaboration in the research of a-C, Dr M. Handrea (BAM-Berlin) and Dr S. Kennou (Univ. Patras) for the XPS measurements and analyses, Prof. J. Robertson (Cambridge) for providing the FCVA-grown a-C samples and Dr Y. Panayiotatos (AUTh) for the preparation of BN samples.

REFERENCES

[1] P.B. Mirkarimi, K.F. McCarty and D.L. Medlin // *Mater.Sci. Engin.* **R21** (1997) 47.
[2] J. Robertson // *Mater. Sci. Eng.* **R37** (2002) 129.
[3] P. Patsalas, S. Logothetidis, S. Kennou and C. Gravalidis // *Thin Solid Films* **428** (2003) 211.
[4] P. Patsalas, M. Handrea, S. Logothetidis, M. Gioti, S. Kennou and W. Kautek // *Diam. Relat. Mater.* **10** (2001) 960.
[5] P.Widmayer, P.Ziemann, S.Ulrich and H. Erhardt // *Diam. Relat. Mater.* **6** (1997) 62.
[6] Y. Panayiotatos, P. Patsalas, C. Charitidis and S. Logothetidis // *Surf. Coat. Tech.* **151 –152** (2002) 155.
[7] Y. Panayiotatos, S. Logothetidis, M. Handrea and W. Kautek // *Diam. Relat. Mater.* (2003), in press.
[8] R.J. Jaccodine and W.A. Schlegel // *J. Appl. Phys.* **37** (1966) 2429.
[9] Y. Panayiotatos, S. Logothetidis, A. Laskarakis, A. Zervopoulou and M. Gioti // *Diam. Relat. Mater.* **11** (2002) 1281.
[10] S. Weissmantel and G. Reisse // *Appl. Surf. Sci.* **154** (2000) 428.
[11] D.H.Berns and M.A.Cappelli // *Appl. Phys. Lett.* **68** (1996) 2711.
[12] D.E.Aspnes // *Thin Solid Films* **89** (1982) 242.
[13] D.A.G.Bruggemann // *Ann. Phys.* **24** (1935) 636.
[14] A.C. Ferrari, A. Libassi, B.K. Tanner, V. Stolojan, J. Yuan, L.M. Brown, S.E. Rodil, B. Kleinsorge and J. Robertson // *Phys. Rev. B* **62** (2000) 11089.
[15] R.Berman and F.Simon // *Z. Electrochem.* **59** (1955) 333.
[16] C.A.Davis // *Thin Solid Films* **226** (1993) 30.
[17] D.R. McKenzie, W.D. McFall W.G. Sainty, C.A. Davis and R.E. Collins // *Diam. Relat. Mater.* **2** (1993) 970.
[18] J.F. Ziegler, J.P. Biersack and U. Littmark, *The Stopping and Range of Ions in Solids* (Pergamon Press,1985); http://www.research.ibm.com/ionbeams.
[19] Y. Lifshitz, S.R. Kasi, J.W. Rabalais and W. Eckstein // *Phys. Rev. B* **41** (1990) 16468.
[20] J.C. Laschovich, R. Giorgi and S. Scaglione // *Appl. Surf. Sci.* **47** (1991) 17.
[21] S.T. Jackson and R.G. Nuzzo // *Appl. Surf. Sci.* **90** (1995) 195.
[22] M.P Seah and W.A. Dench // *Surf. Interf. Anal.* **1** (1979) 2.
[23] C.A. Davis, G.A.J. Amaratunga and K.M. Knowles // *Phys. Rev. Lett.* **80** (1998) 3280.
[24] M. Chhowalla, J. Robertson, C.W. Chen, S.R.P., Silva, C.A. Davis, G.A.J. Amaratunga and W.I. Milne // *J. Appl. Phys.* **81** (1997) 139.

[25] S. Logothetidis, M. Gioti, P. Patsalas and C. Charitidis // *Carbon* **37** (1999) 765.
[26] S. Mohajerzadeh and C.R. Selvakumar // *J. Appl. Phys.* **81** (1997) 3003.
[27] S. Logothetidis, P. Patsalas, M. Gioti, A. Galdikas and L. Pranevicius // *Thin Solid Films* **376** (2000) 56.